# Neural-Network-Based Nonlinear Model Predictive Control for Piezoelectric Actuators

Long Cheng, *Senior Member, IEEE*, Weichuan Liu, Zeng-Guang Hou, *Senior Member, IEEE*, Junzhi Yu, *Senior Member, IEEE*, and Min Tan

***Abstract*—Piezoelectric actuators (PEAs) have been widely used in nanotechnology due to their characteristics of fast response, large mass ratio, and high stiffness. However, hysteresis, which is an inherent nonlinear property of PEAs, greatly deteriorates the control performance of PEAs. In this paper, a nonlinear model predictive control (NMPC) approach is proposed for the displacement tracking problem of PEAs. First, a "nonlinear autoregressive–moving-average with exogenous inputs" (NARMAX) model of PEAs is implemented by multilayer neural networks; second, the tracking control problem is converted into an optimization problem by the principle of NMPC, and then, it is solved by the Levenberg–Marquardt algorithm. The most distinguished feature of the proposed approach is that the inversion model of hysteresis is no longer a necessity, which avoids the inversion imprecision problem encountered in the widely used inversion-based control algorithms. To verify the effectiveness of the proposed modeling and control methods, experiments are made on a commercial PEA product (P-753.1CD, Physik Instrumente), and comparisons with some existing controllers and a commercial proportional–integral–derivative controller are conducted. Experimental results show that the proposed scheme has satisfactory modeling and control performance.**

***Index Terms*—Neural networks, nonlinear autoregressive–moving-average with exogenous inputs (NARMAX), piezoelectric actuator (PEA), predictive control.**

## I. Introduction

NANOTECHNOLOGY has become an important technique in modern manufacturing and process industries during the past decade. Due to its great performance in precise positioning, piezoelectric actuators (PEAs) have been widely used in nanopositioning applications such as computer components [1] and scanning tunneling microscopes [2]. However, hysteresis, which is the dominant nonlinear characteristic in the dynamics of PEAs, can greatly influence the control performance in practical applications. Hysteresis is a kind of memory phenomenon that can be usually found in ferromagnetic materials and piezoelectric ceramics. Because of the existence of hysteresis, the displacement of PEAs depends not only on current control inputs but also on historical inputs. In addition, the frequency of an input signal can also influence the dynamical response of PEAs (i.e., the rate-dependent property).

The modeling of hysteresis is an indispensable part in improving the control performance of PEAs. Several models have been proposed to describe the hysteresis effect, which can be generally classified into two folds, i.e., physics-based models and phenomenon-based models [3]. The physics-based models have a clear physical interpretation. However, they suffer from a complicated structure and a huge computation cost. By contrast, the phenomenon-based models are obtained from experimental data and have relatively simple mathematical descriptions, which become popular in real-world applications.

Here, we briefly review some typical models of hysteresis. **Physics-based model**: In a Preisach model, hysteresis is described by combining an infinite number of Preisach hysteresis operators (each operator has two main parameters to tune) [4]. The difficulty in using a Preisach model lies in dealing with its integral representation. In a Prandtl–Ishlinskii model and its modified models, hysteresis is interpreted by a different operator, i.e., "backlash" [5], [6]. Another widely used model is the Maxwell resistive capacitor model, where hysteresis is modeled by a finite number of elastoslide elements [7]. One common limitation of the aforementioned physics-based models is that they can only represent the hysteresis behavior of PEAs under a fixed-frequency input signal (the so-called *rate-independent* model). **Phenomenon-based model**: The general idea is to use system identification approaches to represent the hysteresis in PEAs. For example, in [8], a linear autoregressive–moving-average (ARMA) approach was employed to model the hysteresis. In [9], a neural-network-based nonlinear model was proposed for hysteresis. An intelligent hysteresis model based on a least square support vector machine was developed in [10], and it was also used for the compensation of the hysteresis behavior. In [11], a recurrent fuzzy model was studied to capture the behaviors of PEAs. It should be noted that, by combining a phenomenon-based hysteresis model and some lower order filters, the combined model can have adaptability with the variations of the input's

Manuscript received November 18, 2014; revised February 25, 2015 and April 25, 2015; accepted June 10, 2015. Date of publication July 10, 2015; date of current version November 6, 2015. This work was supported in part by the National Natural Science Foundation of China under Grant 61422310, Grant 61370032, Grant 61375102, Grant 61225017, and Grant 61421004, and in part by the Beijing Nova Program under Grant Z121101002512066.

The authors are with the State Key Laboratory of Management and Control for Complex Systems, Institute of Automation, Chinese Academy of Sciences, Beijing 100190, China (e-mail: long.cheng@ia.ac.cn).

Color versions of one or more of the figures in this paper are available online at http://ieeexplore.ieee.org.

Digital Object Identifier 10.1109/TIE.2015.2455026

0278-0046 © 2015 IEEE. Personal use is permitted, but republication/redistribution requires IEEE permission.
See http://www.ieee.org/publications_standards/publications/rights/index.html for more information.

frequency, which represents the *rate-dependent* property. Following this idea, the model structure that is composed of a hysteresis submodel and a dynamic submodel (a lower order filter) is commonly adopted in the modeling of PEAs. Under this structure, the hysteresis submodel is independent of the changing rate of the input voltage, and the rate-dependent property is reflected by the dynamic submodel [3]. Therefore, most of the phenomenon-based models belong to the rate-dependent model.

In addition to the modeling of PEAs, how to design effective model-based control algorithms for PEAs is also a research focus in literature. Inversion-based feedforward control is the most popular method, where a high-gain problem in feedback methods is no longer a bottleneck [12]. In this method, the inversion of the hysteresis submodel is obtained first. Then, this inversion is used to compensate for the hysteresis nonlinearity. Once the hysteresis submodel is compensated, the only thing left is designing the feedback controller for the dynamic submodel. For instance, a proportional–integral–derivative (PID) controller combined with an inverse Preisach hysteresis model was proposed to control a PEA [13]. With the inverse Preisach model, a proportional–derivative controller based on the root locus method was introduced into the tracking control of a piezoceramic actuator [14]. In [15], a closest match algorithm for getting the inversion model of hysteresis was used in the open-loop tracking control. However, the tracking performance of the inversion-based method is highly dependent on the precision of the inversion of the hysteresis submodel.

It should be noted that the calculation of the inversion of the hysteresis submodel is not an easy task. The challenge of such methods is the modeling complexity. Meanwhile, the online computation of the inverse hysteresis submodel is an extra burden for the real-time tracking control of PEAs. The inversion calculation methods can be classified into model-based and algorithm-based methods. First, a model-based method is to identify the inversions of some intermediate functions and to use these intermediate functions' inversions to approximate hysteresis models [14]. For instance, the inverse Preisach model does not have an analytical solution, and only a model-based inversion approximation approach can be used. Although an inverse Prandtl–Ishlinskii model can be calculated analytically, the large computation time is still unacceptable [16]. In addition, some existing hysteresis models may not be invertible at all. Second, an algorithm-based method is also used in the identification of inverse hysteresis models [17], [18]. The algorithm-based method usually introduces iterative algorithms to identify inverse hysteresis models. The main limitation of this method is also the large computation cost and the low convergence rate [3].

To deal with the imprecision of inversion models, robust control ideas are introduced into the compensation of hysteresis. For example, an $H_\infty$ controller was designed for the tracking control of PEAs in [19]. However, robust control is a relatively conservative method, which causes difficulties in real-world applications. In recent years, some advanced feedback control methods have been introduced in the field of control of PEAs. In [20], a nonlinear PID controller was used for a compliant nanopositioning stage, and an extended state observer was developed to improve the performance of the PID controller. In [21], a digital sliding-mode controller was introduced in the tracking control of a piezo-driven micropositioning system. This scheme has a rapid implementation because it is based on a linear input–output model of the micropositioning system. In [22], both a least square support vector machine and a relevance vector machine were used to formulate rate-dependent hysteresis models, and these models are then combined with a PID controller, resulting in a model-based feedback controller.

The model predictive control (MPC) method is widely used in industrial applications [23], [24], and it shows great performance and robustness in practice [25]. However, it is rarely applied in the tracking control of PEAs. In [26], an inversion-based MPC method with an integral of the error state variable was proposed for the displacement tracking of PEAs. However, the MPC approach is only used to deal with the dynamic submodel. The hysteresis is described by the Duhem-based model and then compensated by its inversion. Therefore, the controller proposed in [26] still belongs to the inversion-based control category. The imprecision of an inverse hysteresis model dramatically degrades the control performance of PEAs as well. In [27], the MPC method was used in the control of a shape-memory-alloy-based manipulator, which also has the inherent hysteresis nonlinearity.

In this paper, a neural-network-based inversion-free controller is proposed for the displacement tracking control of PEAs. First, a PEA is modeled by cascading a hysteresis submodel and a dynamic submodel. By the results in [28]–[30], this architecture can lead to a rate-dependent model of PEAs. Two "nonlinear ARMA with exogenous inputs" (NARMAX) models are designed to represent the hysteresis submodel and the dynamic submodel, respectively. Both NARMAX models are implemented by multilayer feedforward neural networks. Second, a nonlinear MPC (NMPC) approach is proposed to deal with the displacement tracking problem. The NMPC method can avoid the calculation of the inversion of hysteresis models, which saves the computation resources and is suitable for online control. Following the MPC principle, the tracking control problem is transformed into an optimization problem, where the difference between the desired displacement and the model's predicted displacement is minimized. The Levenberg–Marquardt (LM) algorithm is then introduced to solve the corresponding optimization problem. Finally, to verify the effectiveness of the proposed modeling and control algorithms, experiments were conducted on a commercial PEA product (P-753.1CD, Physik Instrumente, Karlsruhe, Germany). By the experimental results and corresponding comparisons, the tracking performance of the proposed controller is satisfactory.

The rest of this paper is organized as follows. Section II discusses the neural-network-based NARMAX model of PEAs; Section III gives the idea of using NMPC to deal with the displacement tracking problem of PEAs. Experimental verifications and some comparisons are conducted in Section IV, and Section V concludes this paper with final remarks and gives the future work.

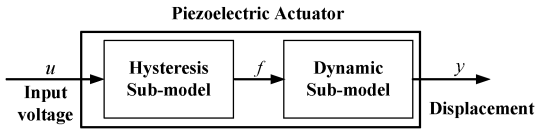


Fig. 1. Schematic of the model of PEAs.

## II. NARMAX-Based Model of PEAs: Multilayer Feedforward Neural Network Approach

Since the behavior of PEAs is dependent on a control input's frequency (the rate-dependent property), a PEA is modeled by cascading a hysteresis submodel and a dynamic submodel, which is shown in Fig. 1. This structure is usually adopted in the modeling of PEAs. Input voltage $u$ acts on the hysteresis submodel, and the output of the hysteresis submodel is an equivalent mechanical force, which is represented by $f$. Subsequently, $f$ acts on the dynamic submodel and then produces the actual displacement $y$ of PEAs. How to identify these two submodels is to be given in the following sections, which is based on the NARMAX idea and the neural network approximation.

NARMAX is a very effective way for nonlinear system identification. It has a great ability of predicting the future output of systems that have complicated nonlinear dynamical characteristics [31]. Hence, two submodels of PEAs can be fitted by NARMAX models. The generic representation of a NARMAX model is given as follows [32]:

$$y(t) = g\left[y(t-1), \ldots, y(t-r), u(t-1), \ldots, u(t-s)\right] \quad (1)$$

where $y(t)$ and $u(t)$ represent the output and input of the NARMAX model, respectively; and integers $r$ and $s$ are the corresponding maximum orders for $y(t)$ and $u(t)$, respectively. How to determine the interconnection among $y(t-1), \ldots, y(t-r), u(t-1), \ldots, u(t-s)$ (i.e., determine nonlinear function $g(\cdot)$) is a challenging job.

Due to their universal approximation ability, neural networks such as a backpropagation neural network and a radial-basis-function neural network have been widely applied in the field of function approximation. This paper adopts a multilayer feedforward neural network to implement the NARMAX representations of the hysteresis submodel and the dynamic submodel as follows:

$$\begin{aligned} f(t) &= g_{\text{hys}}\left[f(t-1), \ldots, f(t-n_a), u(t-1), \ldots, u(t-n_b)\right] \\ y(t) &= g_{\text{dyn}}\left[y(t-1), \ldots, y\left(t-n_a'\right), f(t-1), \ldots, f\left(t-n_b'\right)\right]. \end{aligned} \quad (2)$$

The multilayer feedforward neural networks are used to approximate the unknown nonlinear mappings $g_{\text{hys}}(\cdot)$ and $g_{\text{dyn}}(\cdot)$.

### A. Hysteresis Submodel of PEAs

The hysteresis nonlinearity of PEAs depends not only on current inputs but also on historical inputs. The structure of the multilayer feedforward neural network is shown in Fig. 2. Specifically, this neural network has three layers, i.e., the input layer, the hidden layer, and the output layer. A tangent sigmoid function is chosen as the activation function of the neurons in the hidden layer, whereas a linear unit mapping function is the activation function of the neurons in the input and output layers. The input–output relationship of this neural network can be therefore written as follows:

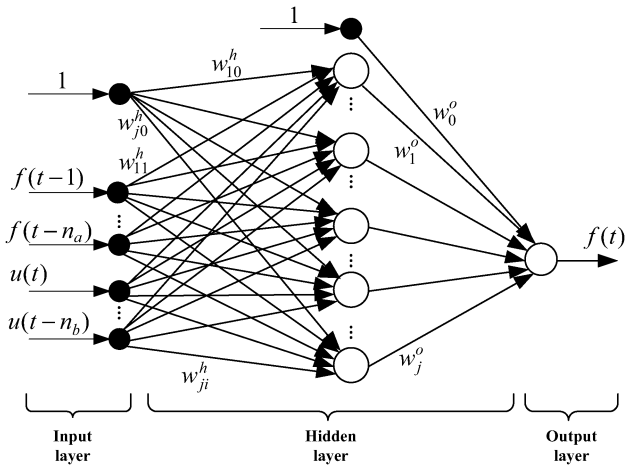


Fig. 2. Neural network structure for the hysteresis submodel.

$$f(t) = \sum_{j=1}^{q} w_j^o \sigma\left(\sum_{i=1}^{p} w_{ji}^h z_i(t) + w_{j0}^h\right) + w_0^o \quad (3)$$

where $p = n_a + n_b$ and $q$ are the numbers of neurons in the input and hidden layers, respectively. $z_i(t)(i = 1, \ldots, p)$ are the inputs of this neural network. According to the structure of the NARMAX model (2), $\{z_1(t), \ldots, z_i(t)\}$ are $\{f(t-1), \ldots, f(t-n_a), u(t), \ldots, u(t-n_b)\}$. $\sigma(\cdot)$ denotes the hyperbolic tangent activation function, and

$$\sigma(x) = \frac{e^{2x}-1}{e^{2x}+1}. \quad (4)$$

For convenience, (3) can be rewritten in a compact form as follows:

$$f(t) = W^o \overline{\sigma}\left(W^h Z(t)\right) \quad (5)$$

where $W^h \in \Re^{q\times(p+1)}$ and $W^o \in \Re^{1\times(q+1)}$ are the weight matrices of the hidden layer and the output layer, respectively, $Z = [1, z_1(t), z_2(t), \ldots, z_p(t)]^T \in \Re^{p+1}$, and $\overline{\sigma}(W^h Z(t)) = [1, \sigma(W_{r_1}^h Z), \sigma(W_{r_2}^h Z), \ldots, \sigma(W_{r_q}^h Z)]^T \in \Re^{q+1}$ ($W_{r_i}^h$ represents the $i$th row of matrix $W^h$).

It is notable that the rate dependence in the PEAs comes from the input voltage with different frequencies. Under the model structure in Fig. 1, the rate dependence is captured by the dynamic submodel [2]. For this reason, the dynamic submodel can be seen as a unit mapping when the frequency of the input voltage is fixed. Hence, the output of the hysteresis submodel, i.e., $f(t)$, can be replaced by the real displacement measurement of the PEAs in the model identification process when the excited signal is of a fixed frequency.

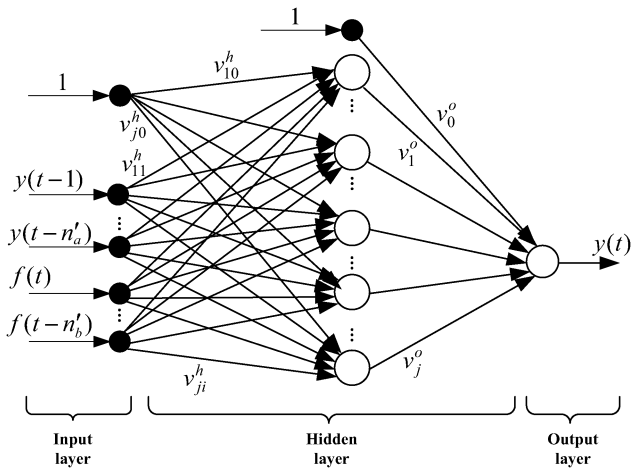


Fig. 3. Neural network structure for the dynamic submodel.

### B. Dynamic Submodel of PEAs

The dynamic submodel of PEAs is usually treated as a linear low-order model [8], [29]. However, by some reports in [33], the dynamic behavior of PEAs is not strictly linear. To improve the accuracy of the dynamic submodel, a multilayer feedforward neural network is introduced to interpret the dynamic submodel, whose structure is shown in Fig. 3. The input–output relationship of this neural network can be written as follows:

$$\begin{aligned} y(t) &= \sum_{j=1}^{q'} v_j^o \sigma\left(\sum_{i=1}^{p'} v_{ji}^h x_i(t) + v_{j0}^h\right) + v_0^o \\ &= V^o \overline{\sigma}\left(V^h X(t)\right) \end{aligned} \tag{6}$$

where the weight matrices and the parameters have the same meanings as those in the hysteresis submodel. $V^h \in \Re^{q' \times (p'+1)}$, and $V^o \in \Re^{1 \times (q'+1)}$; $X = [1, x_1(t), x_2(t), \ldots, x_{p'}(t)]^T \in \Re^{p'+1}$, and $\overline{\sigma}(V^h X) = [1, \sigma(V_{r_1}^h X), \sigma(V_{r_2}^h X), \ldots, \sigma(V_{r_{q'}}^h X)]^T \in \Re^{q'+1}$.

### C. Identification of Hysteresis and Dynamic Submodels

As aforementioned, two different multilayer feedforward neural networks are used to approximate the hysteresis and dynamic submodels, respectively. The main challenge in the identification is to obtain optimal weight matrices. To this end, experiments are first conducted on the PEA to collect some input–output data pairs. Then, the weight matrices are determined in a supervised training fashion.

The hysteresis submodel should be first identified because the identification of the dynamic submodel needs the output data of the hysteresis submodel. An excited signal with a fixed frequency is applied on the PEA. Due to the frequency of the excited signal being fixed, the displacement of the PEAs is equal to the output of the hysteresis submodel. Let the measured data set for training be $S = \{(u(t), d_h(t)) | t = 1, \ldots, N\}$, where $d_h(t)$ is the displacement of the PEAs, $u(t)$ is the fixed-frequency input signal, and $N$ denotes the number of sampled data pairs. Let $W = [W^o, W_{r_1}^h, \ldots, W_{r_q}^h]^T \in \Re^{(q\times(p+1)+1\times(q+1))\times 1}$ be the weight vector for training; then, the optimal $W$ can minimize the mean-square-error criterion as follows:

$$J(W) = \frac{1}{2N}(D_h - F)^T (D_h - F) \tag{7}$$

where $D_h = [d_h(1), d_h(2), \ldots, d_h(N)]^T$, and $F = [f(1), f(2), \ldots, f(N)]^T$. The optimization problem defined by (7) is a nonlinear least square problem, and it can be solved in the following iterative way:

$$W^{(i+1)} = W^{(i)} + \lambda^{(i)} \mu^{(i)} \tag{8}$$

where integer $i$ stands for the index of iteration, $\lambda^{(i)}$ is the step size to control the convergence rate, and $\mu^{(i)}$ is the $i$th *search direction*, which is calculated by training algorithms to make sure that the value of (7) can be descended in each iteration.

In literature, many training algorithms can give a solution to (8). In this paper, the LM training method is employed to train the neural networks due to its rapid convergence and robustness properties [34]. Marquardt gave the following update rule [36] for solving (8):

$$\begin{cases} W^{(i+1)} = W^{(i)} + \mu^{(i)} \\ \left(R\left(W^{(i)}\right) + \lambda^{(i)} I\right) \mu^{(i)} = -G\left(W^{(i)}\right) \end{cases} \tag{9}$$

where $G(W^{(i)}) = \partial J / \partial W$ is the gradient matrix of (7) with respect to $W$. It is well known that the calculation of the inversion of the *Hessian matrix* of (7) is very expensive [35]. For this reason, $R(W^{(i)})$, which is the so-called *Guass–Newton Hessian* matrix, is used to replace the real Hessian matrix. The calculation of $R(W^{(i)})$ can be found in [35]. $\lambda^{(i)}$ should be adjusted in each iteration [36]. Hence, we introduce a modified step in the LM algorithm, which is summarized in Algorithm 1.

**Algorithm 1** Training Method of Multilayer Feedforward Neural Networks for the Hysteresis Submodel and the Dynamic Submodel

1: Choose initial values for $W^{(0)}$ and $\lambda^{(0)}$, and set error tolerance $\epsilon > 0$;
2: Calculate $[R(W^{(i)}) + \lambda^{(i)} I]\mu^{(i)} = -G(W^{(i)})$ to determine search direction $\mu^{(i)}$;
3: Calculate $r^{(i)} = (J(W^{(i)}) - J(W^{(i)} + \mu^{(i)}))/(J(W^{(i)}) - L^{(i)}(W^{(i)} + \mu^{(i)}))$, where $L^{(i)}(W^{(i)} + \mu^{(i)}) = J(W^{(i)}) + \mu^{(i)^T} G(W^{(i)}) + (1/2)\mu^{(i)^T} R(W^{(i)}) \mu^{(i)^T}$;
4: If $r^{(i)} < 0.25$, set $\lambda^{(i)} = 2\lambda^{(i)}$;
5: If $r^{(i)} > 0.75$, set $\lambda^{(i)} = 1/2\lambda^{(i)}$;
6: If $J(W^{(i)} + \mu^{(i)}) < J(W^{(i)})$, then set $W^{(i+1)} = W^{(i)} + \mu^i$, $\lambda^{(i+1)} = \lambda^{(i)}$, and $i = i + 1$;
7: If $|J(W^{(i)} + \mu^{(i)}) - J(W^{(i)})| > \epsilon$, go to 2; otherwise, the algorithm stops.

After obtaining the hysteresis submodel, the dynamic submodel can be identified as well. Since the dynamic submodel describes the rate dependence of the PEAs, the excited signal for its identification is of varied frequencies. In the

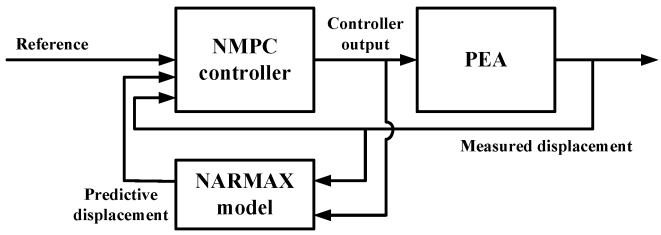


Fig. 4. Schematic of the NMPC method.

identification process, the excited signal is applied on the PEA, and then, the output data of the hysteresis submodel and the real displacement measurement of the PEAs are collected as training data pairs $S = \{(f(t), d_d(t))|t = 1, \ldots, N\}$, where $f(t)$ is the virtual mechanical force generated from the hysteresis submodel, and $d_d(t)$ is the real displacement of the PEAs under the input voltage of varied frequencies.

Let $V = [V^o, V^h_{r_1}, \ldots, V^h_{r_{q'}}]^T \in \Re^{(q'\times(p'+1)+1\times(q'+1))\times 1}$; the optimization problem is

$$\min_V J(V) = \frac{1}{2N}\sum_{i=1}^{N}(d_d(i) - y(i))^2. \tag{10}$$

Then, Algorithm 1 can also be employed to solve the optimization problem defined by (10).

## III. NMPC-Based Displacement Tracking Control of PEAs

Inversion-based control schemes are widely used in the controller design of PEAs. However, obtaining the model's inversion requires huge computation resources. Therefore, an inversion-free controller design method may be a better choice for displacement tracking control. However, this kind of approach is rarely reported in literature. Inspired by this idea, an inversion-free control scheme, i.e., NMPC, is used for the displacement tracking control of PEAs.

To suppress the unknown disturbances in real-time applications, the proposed NMPC method is designed in a finite horizon of prediction, and the basic control schematic is illustrated in Fig. 4. The reference signal is the desired trajectory of the PEAs. The proposed NARMAX model is used as a predictor of the PEA's displacement.

The purpose of tracking control is to minimize the distance between the desired trajectory and the predicted displacement of the PEAs. Meanwhile, the changing rate of the controller's output is another factor of interest. To summarize, the control objective can be written to minimize the following criterion:

$$\begin{aligned} J(U(t)) &= \left[R(t) - \hat{Y}(t)\right]^T \left[R(t) - \hat{Y}(t)\right] + \rho U^T(t)U(t) \\ &= E^T E(t) + \rho U^T(t)U(t) \end{aligned} \tag{11}$$

where $R(t) = [r(t+N_1), \ldots, r(t+N_2)]^T$, $\hat{Y}(t) = [\hat{y}(t+N_1), \ldots, \hat{y}(t+N_2)]^T$, $E(t) = [e(t+N_1), \ldots, e(t+N_2)]^T$, $U(t) = [\Delta u(t), \ldots, \Delta u(t+N_u-1)]^T$, $\Delta u(t) = u(t) - u(t-1)$, and $e(t) = r(t) - \hat{y}(t)$. $\hat{y}(t)$ is the predicted displacement of the PEAs by the NARMAX model proposed in Section II. Integer $N_1 > 0$ denotes the minimum prediction horizon, and integer $N_2 > N_1$ is the maximum prediction horizon; $N_u$ denotes the control horizon, and $r(t)$ denotes the reference signal of the PEAs. To avoid the excessive change in $u(t)$, a penalty term $\rho U^T(t)U(t)$ is added in the objective function, and $\rho > 0$ is the penalty parameter. Before realizing the control scheme, the predicted displacements of the PEAs, i.e., $\hat{Y}(t)$, should be obtained first.

Provided the measured (current and historical) displacements of the PEAs and the NMPC controller's outputs, the predicted displacement of the PEAs can be calculated by the proposed NARMAX as follows:

$$\begin{aligned} \hat{y}(t+k) &= V^o\overline{\sigma}\left(V^h X(t+k)\right) \\ &= V^o\overline{\sigma}\left(V^h\left[1, y(t+k-1), \ldots, y\left(t+k-n'_a\right),\right.\right. \\ &\qquad \left.\left. f(t+k), \ldots, f\left(t+k-n'_b\right)\right]^T\right) \\ &= V^o\overline{\sigma}\left(V^h\left[1, y(t+k-1), \ldots, y\left(t+k-n'_a\right),\right.\right. \\ &\qquad W^o\overline{\sigma}\left(W^h Z(t+k)\right), \ldots, \\ &\qquad \left.\left. W^o\overline{\sigma}\left(W^h Z\left(t+k-n'_b\right)\right)\right]^T\right) \end{aligned} \tag{12}$$

where $k \in \{N_1, \ldots, N_2\}$ is the predicted step index. After obtaining the predicted displacements, the control scheme of the NMPC method can be achieved. Notice that criterion (11) is an optimization problem that can be also solved by the LM algorithm used in Section II-C. However, there is a slight difference compared with the solution to (11). The Hessian matrix of the objective function can be analytically obtained as follows:

$$\begin{aligned} H\left[U^{(i)}\right] &= \frac{\partial^2 J(U)}{\partial U^2} \\ &= \frac{\partial}{\partial U}\left(\frac{\partial Y^T}{\partial U}E(t)\right) + 2\rho\frac{\partial \hat{U}^{(T)}}{\partial U}\frac{\partial \hat{U}}{\partial U}. \end{aligned} \tag{13}$$

Then, we use the real Hessian matrix instead of Guass–Newton Hessian matrix $R(W^{(i)})$ in the LM algorithm. It can be seen that the second term in (13) is positive semidefinite, whereas the positive definiteness of the first term in (13) cannot be guaranteed. Therefore, we take a modified step in the LM algorithm that is summarized in Algorithm 2. Meanwhile, penalty parameter $\rho$ can be chosen to be relatively large to ensure the positive definiteness of $[H(U^{(i)}) + \lambda^{(i)}I]$.

**Algorithm 2** Calculate the NMPC Controller's Output

1: Initialize $\rho > 0$, $\lambda^{(0)}$, and the maximum iteration, and set tolerance $\epsilon > 0$;
2: Try Cholesky factorization on $[H(U^{(i)}) + \lambda^{(i)}I]$, and if the factorization fails (the matrix is not positive definite), set $\lambda^{(i)} = 4\lambda^{(i)}$ and go to 2;
3: Calculate $[H(U^{(i)}) + \lambda^{(i)}I]\mu^{(i)} = -G(U^{(i)})$ to determine search direction $\mu^{(i)}$;

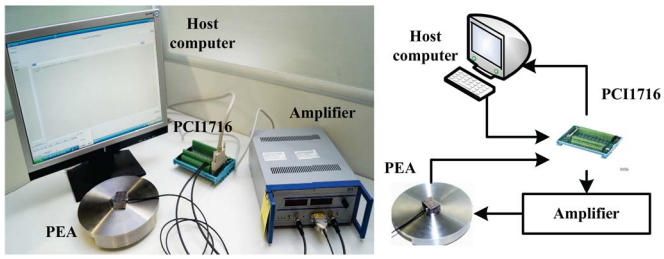


Fig. 5. Experimental setup.

4: Calculate $J(U^{(i)}+\lambda^{(i)})$ and $r^{(i)}=(2J(U^{(i)})-2J(U^{(i)}+\mu^{(i)}))/(\lambda^{(i)}(\mu^{(i)})^T\mu^{(i)}-(\mu^{(i)})^TG[U^{(i)}])$;
5: If $r^{(i)}<0.25$, set $\lambda^{(i)}=2\lambda^{(i)}$;
6: If $r^{(i)}>0.75$, set $\lambda^{(i)}=1/2\lambda^{(i)}$;
7: If $J(U^{(i)}+\mu^T)<J(U^{(i)})$, then set $U^{(i+1)}=U^{(i)}+\mu^i$, $\lambda^{(i+1)}=\lambda^{(i)}$, and $i=i+1$;
8: If $|J(U^{(i)}+\mu^{(i)})-J(U^{(i)})|<\epsilon$ or the maximum iteration number is met, stop the algorithm; otherwise, go to 3.

Algorithm 2 may cost a long time to run over. However, in a real-time application, it must be accomplished in an allowable period. Due to this requirement, a parameter, i.e., the maximum iteration number, is introduced in Algorithm 2.

It should be noted that many other methods can be used to solve the optimization problem generated by the NMPC method. For example, a recurrent neural network is a promising weapon that is featured by its parallel computation nature [37]–[39]. In future work, some efforts are to be made toward solving the NMPC of PEAs by recurrent neural networks.

## IV. Experiments and Discussion

To verify the effectiveness of the proposed modeling and control algorithms, experiments are conducted on a commercial PEA product (P-753.1CD, Physik Instrumente). We set the range of the input voltage from $-10$ to 90 V to avoid possible excess of the PEA's driver. The PEA can perform a high-precision horizontal movement up to 15 $\mu$m. A built-in capacitive displacement sensor is provided for measurement. To implement the connection between the host computer and the PEA, both of them were wired to an input–output data acquisition board (PCI-1716, Advantech, Beijing, China). The sampling time in the following experiments is 0.05 ms. By means of Real-Time Windows Target, the proposed modeling and control algorithms are programmed in the SIMULINK environment. The experimental setup is shown in Fig. 5.

### A. Model Verification and Comparison

The hysteresis submodel should be identified first. Because the hysteresis nonlinearity dominates the performance of PEAs under a low-frequency input voltage [8], an excited sinusoid voltage signal whose frequency is 1 Hz is used to excite the PEA. By considering the whole moving range of the PEAs, the input voltage is set to be $40\sin(2\pi t-0.5\pi)+50$. With the measured displacements and the excited signal, weight matrices

TABLE I
Modeling Performance of the Hysteresis Submodel: The RMS Error and the Maximum (MAX) Error

| the values of $n_a$ and $n_b$ | the RMS modeling error ($\mu$m) | the MAX modeling error ($\mu$m) |
|---|---|---|
| $n_a=0$, $n_b=2$ | 0.5668 | 1.2213 |
| $n_a=3$, $n_b=2$ | 0.0012 | 0.0044 |
| $n_a=5$, $n_b=2$ | 0.0012 | 0.0045 |

TABLE II
Modeling Performance of the Dynamic Submodel: The RMS Error and the Maximum (MAX) Error

| the frequency of the excited signal | the RMS/MAX errors ($\mu$m) ($n'_a=0$ and $n'_b=1$) | the RMS/MAX errors ($\mu$m) ($n'_a=2$ and $n'_b=1$) |
|---|---|---|
| $f=1$ Hz | 0.1015 / 0.1913 | 0.0010 / 0.0164 |
| $f=10$ Hz | 0.1014 / 0.2087 | 0.0013 / 0.0108 |
| $f=50$ Hz | 0.1033 / 0.2981 | 0.0058 / 0.0583 |
| $f=100$ Hz | 0.1059 / 0.3994 | 0.0121 / 0.1066 |
| $f=200$ Hz | 0.2629 / 0.4200 | 0.0355 / 0.2507 |

$W^h$ and $W^o$ can be trained by the algorithm proposed in Section II. The number of hidden-layer neurons in the multilayer feedforward neural network for the hysteresis submodel is determined in a trial-and-error manner, and this number is set to be five in this specific application. To determine the values of integers $n_a$ and $n_b$, a comparison experiment of the hysteresis submodel's modeling performance is given in Table I. The hysteresis property means that the current displacement of the PEAs is relevant with its historical displacements. Therefore, when $n_a=0$ (the hysteresis nonlinearity is only affected by the current input voltage), the modeling performance of the hysteresis submodel is not acceptable (the RMS error is 0.5656 $\mu$m greater than that of the other cases). Furthermore, the models with $n_a\in\{3,4,5\}$ have almost the same model matching. However, with the increase in $n_a$, the computational burden becomes heavier. Therefore, $n_a$ is finally chosen to be three. Furthermore, $n_b=2$ is determined in a similar way.

To identify the dynamic submodel, a mixed sinusoid voltage signal with varied amplitudes and frequencies is applied to the PEA. The excited signal $f$ for the input of the dynamic submodel can be gathered through the obtained hysteresis submodel, and the output of the dynamic submodel is the real displacement of the PEAs. By Algorithm 1, the weight matrices ($V^h$ and $V^o$) of the dynamic submodel are trained as well. The hidden layer of the neural network includes five neurons, and the influences of the selections of $n'_a$ and $n'_b$ on the dynamic submodel are shown in Table II. If $n'_a=0$, the modeling error is obviously greater than that of the model with $n'_a=2$. Furthermore, with the increase in the excited signal's frequency, the model with $n'_a=2$ has the most satisfactory model matching (the RMS error is only 0.0355 $\mu$m for the 200-Hz excited signal). Hence, we set $n'_a=2$ and $n'_b=1$.

To compare the modeling performance between the proposed model and the other models in literature, two comparison experiments are conducted.

*1) Comparison Between Proposed Neural-Network-Based Dynamic Submodel and Linear Dynamic Submodel:* To compare the proposed neural-network-based

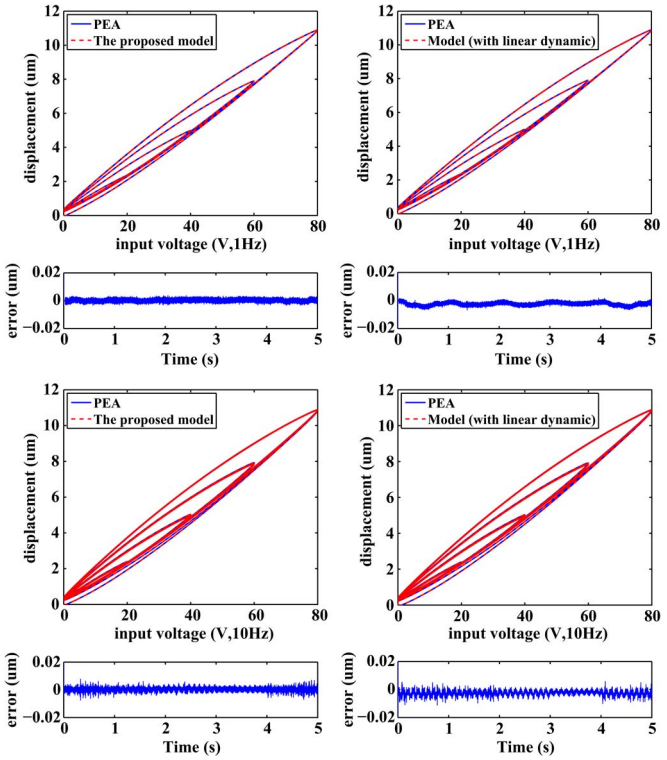


Fig. 6. Comparison experimental results with the low-frequency input voltage.

dynamic submodel with the linear dynamic submodel in literature, a linear ARMA with exogenous inputs (ARMAX)-based model is identified as well. The training data set is the same as the data set used in the identification of the nonlinear dynamic submodel. The LM algorithm is used to identify the linear dynamic submodel in an offline manner. The obtained linear model can be written in the following form of a discrete transfer function:

$$G(Z) = \frac{0.4931z - 0.2931}{z^2 - 1.504z + 0.7041}.$$

The hysteresis submodel is cascaded with the neural-network-based dynamic submodel and the linear dynamic submodel, resulting in the proposed model and the model with linear dynamics, respectively. As shown in Fig. 6, two sinusoid signals with different frequencies (1 and 10 Hz, respectively) act on the proposed model, the model with the linear dynamic submodel, and the real PEA. In this low-frequency setup, the fitting performance of the proposed model and that of the model with the linear dynamics are almost the same. These results suggest that both models have a good ability of matching the real behavior of PEAs with the low-frequency input voltage. However, the results with the input voltage of high frequencies (50, 100, and 200 Hz) are much different, which are given in Fig. 7. For the 200-Hz excited sinusoid signal, the modeling error is between $-0.1830$ and $0.1394$ $\mu$m. By contrast, with the linear dynamic submodel, the modeling error is between $-0.4537$ and $0.4294$ $\mu$m. From the experimental results, with the increase in the input frequency, the proposed nonlinear

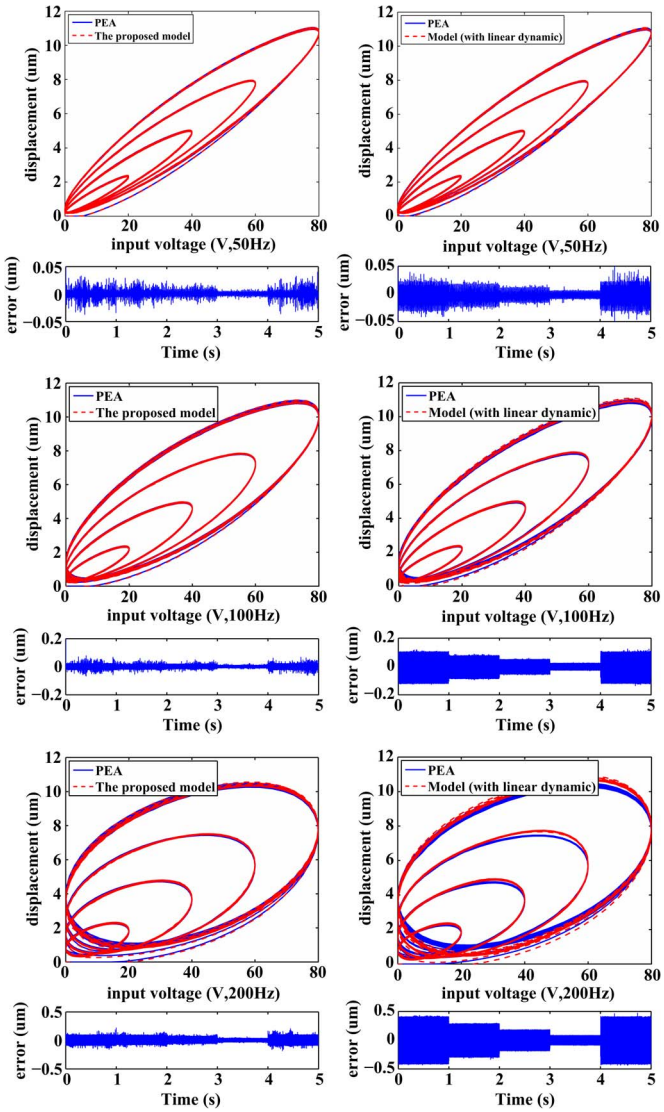


Fig. 7. Comparison experimental results with the high-frequency input voltage.

dynamic submodel has better modeling performance than the linear model.

*2) Comparison Between Proposed Model and Duhem-Based Model:* To compare with the physics-based model, the Duhem-based model is employed to compare with the proposed NARMAX-based model. The comparison results are given in Table III. For the excited sinusoid signal with 200 Hz, the RMS error of the proposed model is 0.1013 $\mu$m less than that of the Duhem-based model. In addition, the MAX error is 0.0268 $\mu$m less than the Duhem-based model. Therefore, the proposed method has better modeling performance than the Duhem-based model.

## B. Verification of NMPC Algorithm

The proposed NMPC method is used for the displacement tracking control of the PEAs. To verify the performance of the NMPC method under reference signals with different frequencies, some mixed sinusoid waves with different frequencies are

TABLE III
MODELING PERFORMANCE COMPARISON BETWEEN THE PROPOSED MODEL AND THE DUHEM-BASED METHOD: THE RMS ERROR AND THE MAXIMUM (MAX) ERROR

| the frequency of excited signals | the proposed model's RMS/MAX errors ($\mu$m) | the Duhem-based model's RMS/MAX errors ($\mu$m) |
|---|---|---|
| $f = 1$ Hz | 0.0022 / 0.0079 | 0.0163 / 0.0926 |
| $f = 10$ Hz | 0.0019 / 0.0152 | 0.0148 / 0.0899 |
| $f = 50$ Hz | 0.0051 / 0.0519 | 0.0160 / 0.1007 |
| $f = 100$ Hz | 0.0101 / 0.1005 | 0.0169 / 0.1414 |
| $f = 150$ Hz | 0.0146 / 0.1798 | 0.0175 / 0.1812 |
| $f = 200$ Hz | 0.0187 / 0.1695 | 0.1200 / 0.1963 |

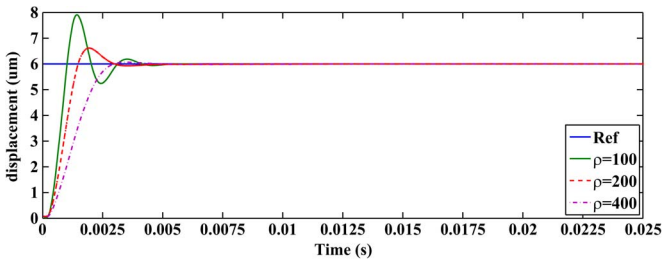


Fig. 8. Tracking performance of PEAs under the step reference with different $\rho$.

used as the desired tracking trajectories. By the obtained PEA's model, the NMPC method has been programmed in a real-time controller.

The maximum iteration number in Algorithm 2 is an important parameter for the NMPC method. The control performance could be improved with the increase in the maximum iteration number. However, it will take a longer time for the calculation of Algorithm 2 if the maximum iteration number is too large. There is a tradeoff between the control performance and the efficiency, and the maximum iteration number is chosen to be five in this paper. Moreover, $N_1$, $N_2$, and $\rho$ in Algorithm 2 are set to be 1, 7, and 50, respectively.

The step responses of the PEA with different $\rho$ are given in Fig. 8. With the increase in $\rho$, the overshoot of the PEA is reduced. Meanwhile, the rising time becomes slightly longer because the large penalty parameter $\rho$ results in a relatively small control effort.

Next, the tracking experiments under the sinusoid trajectories of different frequencies (1, 5, 10, and 50 Hz) are made. As shown in Figs. 9 and 10, the real displacements of the PEAs can track the reference trajectories well. This is because the errors caused by the inversion calculation can be avoided since the proposed NMPC method is an inversion-free method. Meanwhile, the NMPC method is based on the feedback structure so that the unknown disturbance can be rejected. By taking these advantages, the tracking errors can be reduced into a satisfactory range by the proposed NMPC method.

Fig. 11 gives the result of tracking the mixed reference signal that is composed of three sinusoid waves. For the reference that has different amplitudes and varied frequencies from 5 to 10 Hz, the range of the tracking errors is between $-0.03$ and 0.02 $\mu$m in the steady-state phase. The rising time of the control system is also acceptable. For the reference with 10–50 Hz, the

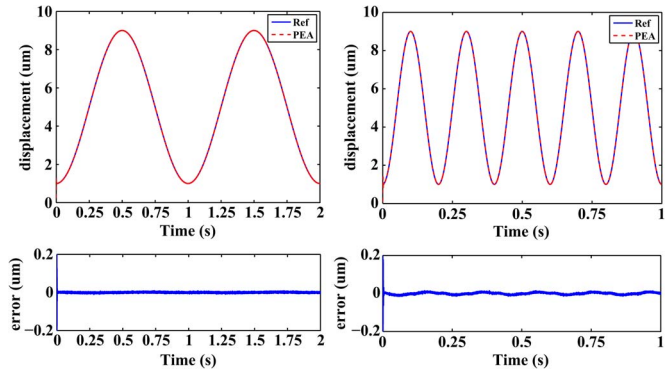


Fig. 9. Tracking performance of the PEAs under 1- and 5-Hz references.

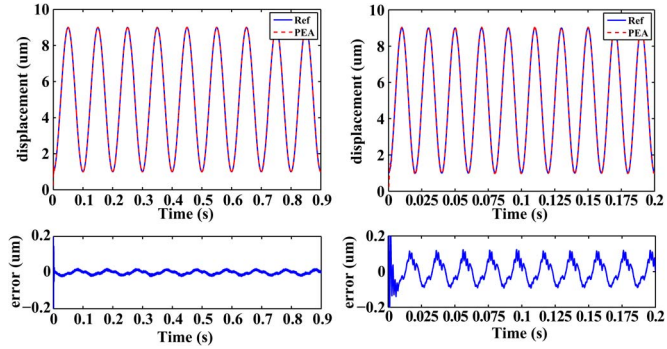


Fig. 10. Tracking performance of the PEAs under 10- and 50-Hz references.

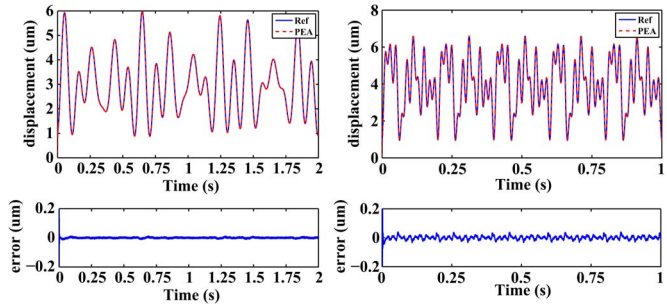


Fig. 11. Tracking performance of the PEAs under a mixed-frequency reference. (Left) 5–10 Hz. (Right) 10–50 Hz.

tracking errors can be still reduced to a small neighborhood of the origin.

In addition, we find that the tracking performance of the proposed NMPC method could be improved when the sampling time of the PEAs is decreased. However, the decrease in the sampling time is a great challenge for the hardware because the proposed algorithm may not be implemented in a very short sampling period. Therefore, there is also a tradeoff between the performance and the implementation.

To further study the control performance of the proposed NMPC method, two comparison experiments are conducted on the PEA.

*1) Comparison Between Proposed Method and Commercial PID Controller:* The commercial PID controller is

TABLE IV
TRACKING PERFORMANCE COMPARISON BETWEEN THE PROPOSED METHOD AND THE COMMERCIAL PID CONTROLLER (WITHOUT LOADS): THE RMS ERROR AND THE MAXIMUM (MAX) ERROR

| the frequency of references | the proposed method's RMS/MAX tracking errors ($\mu$m) | the commercial PID controller's RMS/MAX tracking errors ($\mu$m) |
|---|---|---|
| $f = 1$ Hz | 0.0019 / 0.0064 | 0.0600 / 0.0743 |
| $f = 5$ Hz | 0.0038 / 0.0076 | 0.3032 / 0.4151 |
| $f = 10$ Hz | 0.0087 / 0.0144 | 0.5981 / 0.8295 |
| $f = 20$ Hz | 0.0190 / 0.0289 | 1.1479 / 1.6158 |
| $f = 40$ Hz | 0.0421 / 0.0607 | 2.0639 / 2.9290 |
| $f = 50$ Hz | 0.0552 / 0.0791 | 2.4080 / 3.4197 |
| $f = 100$ Hz | 0.1187 / 0.2740 | 3.9783 / 6.4517 |
| $f = 150$ Hz | 0.3101 / 0.6284 | 4.6363 / 7.7484 |
| $f = 200$ Hz | 0.5315 / 0.9559 | 5.1080 / 8.6671 |

provided by Physik Instrumente, and it is embedded in the PEA's hardware. The tracking reference is defined as $r(t) = 4\sin(2\pi ft - (\pi/2)) + 4$. The RMS tracking error and the MAX tracking error of both controllers are given in Table IV. For the 50-Hz reference, the RMS tracking error is 2.3528 $\mu$m less than that of the commercial PID controller. In addition, the MAX error of the proposed method has very few changes with the increase in the excited signals' frequencies. This implies that the proposed method can deal with the rate-dependent property of the PEAs. By contrast, the MAX error of the commercial PID controller has an apparent increase under different references. When the frequency of the reference signal increases up to 100 Hz, the tracking performance of the proposed method relatively degrades. This deterioration is possibly caused by the precision of the neural-network-based PEA model. In Table III, it can be seen that the modeling error increases as the frequency of the reference signal increases up to 100 Hz. However, even in the high-frequency case, the proposed algorithm still outperforms the commercial PID algorithm.

The aforementioned experiment is made when the PEA has no load. The following comparison experiments are made with the consideration of external loads. The model of the PEAs is identified in the no-load situation. Moreover, the 10- and 50-Hz sinusoid signals are chosen as the tracking references. The comparison results are given in Table V. The NMPC method has satisfactory tracking performance with different loads on the PEA. In addition, compared with the commercial PID controller, better tracking performance can be found. In the best case (the 10-Hz sinusoid reference), the RMS error of the NMPC method is 0.5889 $\mu$m less than that of the commercial PID controller. Moreover, the MAX error of the NMPC method is obviously smaller. When the reference's frequency is increased, the commercial PID controller has deteriorated tracking performance (the RMS error is increased by at least 1.8088 $\mu$m). By contrast, the NMPC method still has good tracking performance (the RMS error is only increased by about 0.0467 $\mu$m). These results imply that the NMPC method could deal with the external loads on the PEA. In addition, it can be seen that the MAX error at $f = 50$ Hz without loads is bigger than the error at the same frequency with loads. This phenomenon is mainly caused by the noise of the PEA's built-in displacement sensor. Through several experimental tests, we find that the noise's amplitude is around 2 nm. Meanwhile, in Tables IV and V, the maximum difference between the MAX error at $f = 50$ Hz without loads and the MAX error at $f = 50$ Hz with loads is only 0.8 nm, which is within the noise's amplitude.

TABLE V
TRACKING PERFORMANCE COMPARISON BETWEEN THE PROPOSED METHOD AND THE COMMERCIAL PID CONTROLLER (WITH DIFFERENT LOADS): THE RMS ERROR AND THE MAXIMUM (MAX) ERROR

| $f = 10$ Hz | the proposed method's RMS/MAX errors ($\mu$m) | the commercial PID controller's RMS/MAX errors ($\mu$m) |
|---|---|---|
| $m_d = 260g$ | 0.0086 / 0.0153 | 0.5974 / 0.8295 |
| $m_d = 360g$ | 0.0088 / 0.0150 | 0.5975 / 0.8297 |
| $m_d = 460g$ | 0.0087 / 0.0153 | 0.5975 / 0.8299 |
| $m_d = 560g$ | 0.0088 / 0.0147 | 0.5975 / 0.8302 |
| $m_d = 660g$ | 0.0088 / 0.0146 | 0.5975 / 0.8299 |
| $m_d = 760g$ | 0.0088 / 0.0149 | 0.5977 / 0.8301 |
| $f = 50$ Hz | the proposed method's RMS/MAX errors ($\mu$m) | the commercial PID controller's RMS/MAX errors ($\mu$m) |
| $m_d = 260g$ | 0.0556 / 0.0787 | 2.4086 / 3.4234 |
| $m_d = 360g$ | 0.0556 / 0.0784 | 2.4079 / 3.4256 |
| $m_d = 460g$ | 0.0556 / 0.0787 | 2.4076 / 3.4306 |
| $m_d = 560g$ | 0.0555 / 0.0789 | 2.4070 / 3.4241 |
| $m_d = 660g$ | 0.0555 / 0.0783 | 2.4069 / 3.4316 |
| $m_d = 760g$ | 0.0555 / 0.0787 | 2.4065 / 3.4335 |

TABLE VI
COMPARISON BETWEEN THE NMPC METHOD AND THE METHOD IN [26]

| Reference frequency | The method in [26] | The NMPC |
|---|---|---|
| $f = 1$ Hz | 0.0083 $\mu$m | 0.0025 $\mu$m |
| $f = 10$ Hz | 0.0201 $\mu$m | 0.0096 $\mu$m |
| $f = 50$ Hz | 0.1669 $\mu$m | 0.0570 $\mu$m |

*2) Comparison With Method Proposed in [26]:* The experimental results are listed in Table VI. The tracking reference is defined as $r(t) = 5\sin(2\pi ft - (\pi/2)) + 5$. It can be seen that the NMPC method has better tracking performance than the method in [26]. In the best case, the RMS error is 0.1099 $\mu$m less than the error of the method in [26].

## V. CONCLUSION AND FUTURE WORK

PEAs are widely used in nanotechnology. The modeling and control of PEAs have drawn great attention in the literature. In particular, the displacement tracking control of PEAs is of great significance in practical applications. In this paper, an NMPC controller, which is an inversion-free method, has been proposed to solve the tracking control problem of PEAs. As the predictor of a PEA's displacement, the PEA's dynamical model is constructed by multilayer feedforward neural networks and identified by the LM algorithm. By the principle of MPC, the tracking control problem is transformed into an optimization problem. Compared with inversion-based control schemes, the NMPC method can directly use a nonlinear neural-network-based model and obtain a proper control action by solving the

corresponding optimization problems. To verify the effectiveness of the proposed modeling and control methods, experiments are conducted on a commercial PEA product through the SIMULINK program. Experimental results show that the proposed NARMAX model could fit the PEA's dynamical behavior well under excited signals with different frequencies and amplitudes. Furthermore, the proposed NMPC controller has better tracking performance than the existing method in [25] and the commercial PID controller.

Although a cascaded model structure is widely used in the control of PEAs, it has to identify two submodels to approximate the rate-dependent hysteresis behavior. If we can use just one intelligent unit (e.g., neural networks and fuzzy systems) to model the rate-dependent hysteresis, the computational burden of the identification can be reduced significantly. In addition, the method proposed in this paper requires solving a complicated nonlinear programming problem, and the MPC law does not have an analytical form. Some preliminary attempts toward obtaining an explicit MPC controller have been made in [40]–[42]. In the future, more studies are to be conducted to further improve the performance of the MPC-based control scheme.

## REFERENCES


[1] W. Yang, S.-Y. Lee, and B.-J. You, "A piezoelectric actuator with a motion-decoupling amplifier for optical disk drives," *Smart Mater. Struct.*, vol. 19, no. 6, May 2010, Art. ID. 065027.

[2] S. Devasia, E. Eleftheriou, and S. O. R. Moheimani, "A survey of control issues in nanopositioning," *IEEE Trans. Control Syst. Technol.*, vol. 15, no. 5, pp. 802–823, Sep. 2007.

[3] J. Y. Peng and X. B. Chen, "A survey of modeling and control of piezoelectric actuators," *Modern Mech. Eng.*, vol. 3, no. 1, pp. 1–20, Feb. 2013.

[4] I. D. Mayergoyz and G. Friedman, "Generalized Preisach model of hysteresis," *IEEE Trans. Magn.*, vol. 24, no. 1, pp. 212–217, Jan. 1988.

[5] K. Kuhnen and F. Previdi, "Modeling, identification and compensation of complex hysteretic nonlinearities: A modified Prandtl–Ishlinskii approach," *Eur. J. Control*, vol. 9, no. 4, pp. 407–421, 2003.

[6] G. Y. Gu, L. M. Zhu, and C. Y. Su, "Modeling and compensation of asymmetric hysteresis nonlinearity for piezoceramic actuators with a modified Prandtl–Ishlinskii model," *IEEE Trans. Ind. Electron.*, vol. 61, no. 3, pp. 1583–1595, Mar. 2014.

[7] T.-J. Yeh, S.-W. Lu, and T.-Y. Wu, "Modeling and identification of hysteresis in piezoelectric actuators," *Trans. ASME, J. Dyn. Syst. Meas. Control*, vol. 128, no. 2, pp. 189–196, May 2005.

[8] Y. Cao and X. B. Chen, "A novel discrete ARMA-based model for piezoelectric actuator hysteresis," *IEEE/ASME Trans. Mechatronics*, vol. 17, no. 4, pp. 737–744, Aug. 2012.

[9] L. Deng and Y. H. Tan, "Modeling hysteresis in piezoelectric actuators using NARMAX models," *Sens. Actuators A, Phys.*, vol. 149, no. 1, pp. 106–112, Jan. 2009.

[10] Q. Xu, "Identification and compensation of piezoelectric hysteresis without modeling hysteresis inverse," *IEEE Trans. Ind. Electron.*, vol. 60, no. 9, pp. 3927–3937, Sep. 2013.

[11] C. Wen and M. Cheng, "Development of a recurrent fuzzy CMAC with adjustable input space quantization and self-tuning learning rate for control of a dual-axis piezoelectric actuated micro motion stage," *IEEE Trans. Ind. Electron.*, vol. 60, no. 11, pp. 5105–5115, Nov. 2013.

[12] K. K. Leang and S. Devasia, "Feedback-linearized inverse feedforward for creep, hysteresis, and vibration compensation in AFM piezoactuators," *IEEE Trans. Control Syst. Technol.*, vol. 15, no. 5, pp. 927–935, Sep. 2007.

[13] P. Ge and M. Jouaneh, "Tracking control of a piezoceramic actuator," *IEEE Trans. Control Syst. Technol.*, vol. 4, no. 3, pp. 209–216, May 1996.

[14] G. Song, J. Q. Zhao, X. Q. Zhou, and J. A. De Abreu-García, "Tracking control of a piezoceramic actuator with hysteresis compensation using inverse Preisach model," *IEEE/ASME Trans. Mechatronics*, vol. 10, no. 2, pp. 198–209, Apr. 2005.

[15] X. Tan, R. Venkataraman, and P. S. Krishnaprassad, "Control of hysteresis: Theory and experimental results," Pentagon, Washington, DC, USA, Tech. Rep. A687934, 2001.

[16] M. A. Janaideh, S. Rakheja, and C. Y. Su, "An analytical generalized Prandtl–Ishlinskii model inversion for hysteresis compensation in micropositioning control," *IEEE/ASME Trans. Mechatronics*, vol. 16, no. 4, pp. 734–744, Aug. 2011.

[17] R. Venkataraman and P. S. Krishnaprasad, "Approximate inversion of hysteresis: Theory and numerical results," in *Proc. 39th IEEE Conf. Decision Control*, Sydney Australia, Dec. 2000, pp. 4448–4454.

[18] J. Y. Peng and X. B. Chen, "$H_2$-optimal digital control of piezoelectric actuators," *Proc. 8th World Congr. Intell. Control Autom.*, Jinan China, Jul. 2010, pp. 3684–3690.

[19] A. Sebastian and S. M. Salapaka, "Design methodologies for robust nanopositioning," *IEEE Trans. Control Syst. Technol.*, vol. 13, no. 6, pp. 868–876, Nov. 2005.

[20] H. Tang and Y. Li, "Development and active disturbance rejection control of a compliant micro/nano-positioning piezo-stage with dual mode," *IEEE Trans. Ind. Electron.*, vol. 61, no. 3, pp. 1475–1492, Mar. 2014.

[21] Q. Xu, "Digital sliding-mode control of piezoelectric micropositioning system based on input–output model," *IEEE Trans. Ind. Electron.*, vol. 61, no. 10, pp. 5517–5526, Oct. 2014.

[22] P. K. Wong, Q. S. Xu, C. M. Vong, and H. C. Wong, "Rate-dependent hysteresis modeling and control of a piezostage using online support vector machine and relevance vector machine," *IEEE Trans. Ind. Electron.*, vol. 59, no. 4, pp. 1988–2001, Apr. 2012.

[23] J. B. Rawlings and D. Q. Mayne, *Model Predictive Control: Theory and Design*. Madison, WI, USA: Nob Hill, 2009.

[24] P. Tatjewski, *Advanced Control of Industrial Processes, Structures and Algorithms*. London, U.K.: Springer-Verlag, 2007.

[25] E. F. Camacho and C. Bordons, *Model Predictive Control*. London, U.K.: Springer-Verlag, 1999.

[26] Y. Cao, L. Cheng, X. B. Chen, and J. Y. Peng, "An inversion-based model predictive control with an integral-of-error state variable for piezoelectric actuators," *IEEE/ASME Trans. Mechatronics*, vol. 18, no. 3, pp. 895–904, Jun. 2013.

[27] N. Nikdel, P. Nikdel, M. A. Badamchizadeh, and I. Hassanzadeh, "Using neural network model predictive control for controlling shape memory alloy-based manipulator," *IEEE Trans. Ind. Electron.*, vol. 61, no. 3, pp. 1394–1401, Mar. 2014.

[28] H. J. M. T. S. Adriaens, W. L. de Koning, and R. Banning, "Modeling piezoelectric actuators," *IEEE/ASME Trans. Mechatronics*, vol. 5, no. 4, pp. 331–341, Dec. 2000.

[29] G. M. Clayton, S. Tien, A. J. Fleming, S. O. R. Moheimani, and S. Devasia, "Inverse-feedforward of charge-controlled piezopositioners," *Mechatronics*, vol. 18, no. 5, pp. 273–281, Jun. 2008.

[30] J. Yi, S. Chang, and Y. Shen, "Disturbance-observer-based hysteresis compensation for piezoelectric actuators," *IEEE/ASME Trans. Mechatronics*, vol. 14, no. 4, pp. 456–464, Aug. 2009.

[31] Y. Gao and J. E. Meng, "NARMAX time series model prediction: Feedforward and recurrent fuzzy neural network approaches," *Fuzzy Sets Syst.*, vol. 150, no. 2, pp. 331–350, Mar. 2005.

[32] S. Chen and S. A. Billings, "Representation of non-linear systems: The NARMAX model," *Int. J. Control*, vol. 49, no. 3, pp. 1012–1032, Oct. 1999.

[33] X. B. Chen, Q. S. Zhang, D. Kang, and W. J. Zhang, "On the dynamics of piezoelectric positioning systems," *Rev. Sci. Instrum.*, vol. 79, no. 11, Oct. 2008, Art. ID. 116 101.

[34] R. Fletcher, *Practical Methods of Optimization*. Hoboken, NJ, USA: Wiley, 1987.

[35] M. Norgaard, O. Ravn, N. K. Poulsen, and L. K. Hansen, *Neural Networks for Modelling and Control of Dynamic Systems*. New York, NY, USA: Springer-Verlag, 2000.

[36] D. Marquardt, "An algorithm for least-squares estimation of nonlinear parameters," *SIAM J. Appl. Math.*, vol. 11, no. 2, pp. 431–441, 1963.

[37] Z. Yan and J. Wang, "Model predictive control of nonlinear systems with unmodeled dynamics based on feedforward and recurrent neural networks," *IEEE Trans. Ind. Informat.*, vol. 8, no. 4, pp. 746–756, Nov. 2012.

[38] M. Lawrynczuk, *Computationally Efficient Model Predictive Control Algorithms: A Neural Network Approach*. Basel, Switzerland: Springer-Verlag, 2014.

[39] L. Cheng, Z.-G. Hou, and M. Tan, "Constrained multi-variable generalized predictive control using a dual neural network," *Neural Comput. Appl.*, vol. 16, no. 6, pp. 505–512, Sep. 2007.

[40] W. Liu, L. Cheng, Z.-G. Hou, J. Yu, and M. Tan, "An inversion-free predictive controller for piezoelectric actuators based on a dynamic linearized neural network model," *IEEE/ASME Trans. Mechatronics*, to be published, DOI: 10.1109/TMECH.2015.2431819.
[41] W. Liu, L. Cheng, Z.-G. Hou, and M. Tan, "An inversion-free model predictive control with error compensation for piezoelectric actuators," in *Proc. Amer. Control Conf.*, Chicago, IL, USA, Jul. 2015, pp. 5489–5494.
[42] W. Liu, L. Cheng, H. Wang, Z.-G. Hou, and M. Tan, "An inversion-free fuzzy predictive control for piezoelectric actuators," in *Proc. 27th Chin. Control Decis. Conf.*, Qingdao China, May 2015, pp. 959–964.

**Long Cheng** (SM'14) received the B.S. degree (with honors) in control engineering from Nankai University, Tianjin, China, in July 2004 and the Ph.D. degree (with honors) in control theory and control engineering from the Chinese Academy of Sciences, Beijing, China, in July 2009.

From February 2010 to September 2010, he was a Postdoctoral Research Fellow with the Department of Mechanical Engineering, College of Engineering, University of Saskatchewan, Saskatoon, SK, Canada. From September 2010 to March 2011, he was a Postdoctoral Research Fellow with the Department of Mechanical and Industrial Engineering, College of Engineering, Northeastern University, Boston, MA, USA. From December 2013 to March 2014, he was a Visiting Scholar with the Department of Electrical and Computer Engineering, Bourns College of Engineering, University of California Riverside, Riverside, CA, USA. Currently, he is a Professor with the State Key Laboratory of Management and Control for Complex Systems, Institute of Automation, Chinese Academy of Sciences. He is the author or coauthor of more than 50 technical papers published in peer-refereed journals and prestigious conference proceedings. His current research interests include the intelligent control of smart materials, the coordination of multiagent systems, and neural networks and their applications to robotics.

Dr. Cheng is an Editorial Board Member of *Neurocomputing* and the *International Journal of Systems Science*.

**Weichuan Liu** received the B.E. degree in control engineering from the North China University of Technology, Beijing, China, in July 2013. He is currently working toward the Ph.D. degree in control theory and control engineering in the State Key Laboratory of Management and Control for Complex Systems, Institute of Automation, Chinese Academy of Sciences, Beijing, China.

His research interests include predictive control, intelligent control, and nanorobots/microrobots.

**Zeng-Guang Hou** (SM'09) received the B.E. and M.E. degrees in electrical engineering from Yanshan University (formerly Northeast Heavy Machinery Institute), Qinhuangdao, China, in 1991 and 1993, respectively, and the Ph.D. degree in electrical engineering from the Beijing Institute of Technology, Beijing, China, in 1997.

He is currently a Professor with the State Key Laboratory of Management and Control for Complex Systems, Institute of Automation, Chinese Academy of Sciences, Beijing, China. His current research interests include neural networks, optimization algorithms, robotics, and intelligent control systems.

Dr. Hou is an Associate Editor of the IEEE TRANSACTIONS ON CYBERNETICS and an Editorial Board Member of *Neural Networks*.

**Junzhi Yu** (SM'14) received the B.E. degree in safety engineering and the M.E. degree in precision instruments and mechanology from the North China Institute of Technology, Taiyuan, China, in 1998 and 2001, respectively, and the Ph.D. degree in control theory and control engineering from the Chinese Academy of Sciences, Beijing, China, in 2003.

He is currently a Professor with the State Key Laboratory of Management and Control for Complex Systems, Institute of Automation, Chinese Academy of Sciences. He is the author or coauthor of more than 100 journal and conference papers. His research interests include biomimetic robots, intelligent control, and intelligent mechatronic systems.

Dr. Yu is an Associate Editor of the IEEE/ASME TRANSACTIONS ON MECHATRONICS.

**Min Tan** received the B.S. degree in control engineering from Tsinghua University, Beijing, China, in 1986 and the Ph.D. degree in control theory and control engineering from the Chinese Academy of Sciences, Beijing, China, in 1990.

He is a Professor with the State Key Laboratory of Management and Control for Complex Systems, Institute of Automation, Chinese Academy of Sciences. His research interests include advanced robot control, multirobot systems, biomimetic robots, and manufacturing systems.